Electrochimica Acta 84 (2012) 187–201

Contents lists available at SciVerse ScienceDirect

Electrochimica Acta

journal homepage: www.elsevier.com/locate/electacta

Review article

Overview of recent developments in oxygen reduction electrocatalysis

Masahiro Watanabe*, Donald A. Tryk, Mitsuru Wakisaka, Hiroshi Yano, Hiroyuki Uchida

Fuel Cell Nanomaterials Center and Clean Energy Research Center, University of Yamanashi, Kofu, Japan

ARTICLE INFO

Article history:
Received 14 February 2012
Received in revised form 4 April 2012
Accepted 6 April 2012
Available online 13 April 2012

Keywords:
Fuel Cell
PEFC
Cathode catalysts
Electrocatalysis
Platinum alloy

ABSTRACT

We review a small selection of recent fundamental and applied results related to the electrocatalysis of the oxygen reduction reaction in acid electrolytes, including polymer electrolytes. There have been a number of promising developments, which may lead to advances at the practical level in polymer electrolyte fuel cells.

© 2012 Elsevier Ltd. All rights reserved.

Contents

1. Introduction

The widespread usage of fuel cell-based electric vehicles (FECVs) based on polymer electrolyte fuel cells (PEFCs), as well as stationary systems for residential use, will depend on whether or not we can meet the necessary requirements for performance, durability and cost. Consumers care more about this performance–durability–cost (PDC) "equation" than they care about what is "under the hood." Therefore, fuel cells must inevitably compete for their place in the future energy market. Even the fuel cell's intrinsic advantage of long-range operation compared to batteries has recently been eroded as the range of battery-powered EVs has improved. In the present review, we will examine some of the important recent research developments that may have an impact on the future PDC equation, with a focus on the cathode electrocatalyst.

The oxygen cathode in the PEFC has experienced an ever-increasing level of scrutiny during the last four years, which shows no sign of leveling off. Even as the automotive industry is making plans to put large numbers of fuel cell powered cars on roads over the next four years, researchers are focusing their efforts on this critical component of the cell. At present, the most promising near-term electrocatalysts for the oxygen reduction reaction (ORR) appear to be the platinum-based bimetallic systems, and it is likely that these will be used in electric vehicles in the future, but

* Corresponding author.
E-mail address: m-watanabe@yamanashi.ac.jp (M. Watanabe).

0013-4686/$ – see front matter © 2012 Elsevier Ltd. All rights reserved.
http://dx.doi.org/10.1016/j.electacta.2012.04.035

many researchers believe that it is still possible to make significant improvements, perhaps with radically new types of materials.

Japan's New Energy and Industrial Technology Development Organization (NEDO) has proposed fuel cell targets for fuel cell performance, durability and cost for 2015: 51% efficiency based on the higher heating value (HHV) of the fuel, i.e., natural gas, with all of the products being cooled to room temperature, 60% efficiency based on the lower heating value (LHV) of the fuel, i.e., the products, such as water, not being cooled to room temperature, a lifetime of greater than 5000 h and a fuel cell system cost of 1,000,000 JPY (13,000 USD), i.e., 10,000 JPY/kW ($130 kW^{-1}) for a 100 kW engine, based on a volume production of 500,000 vehicles [1]. The European Hydrogen and Fuel Cell Technology Platform (HFP) has proposed similar targets. The US Department of Energy (DOE) has also proposed similar 2015 targets of a lifetime of 5000 h, which translates to 150,000 miles (241,400 km), assuming an average speed of 30 miles h^{-1} (48.3 km h^{-1}). The cost target for the stack itself is proposed to be $30 kW^{-1} (2300 yen kW^{-1}). The status as of mid-2011 was given as $49 kW^{-1} (3800 yen kW^{-1}) [2].

The recent developments in battery-powered electric vehicles, for example, the Nissan Leaf (175 km, 109 mile range) and the Tesla Roadster (320 km, 200 mile range) per charge, are now putting pressure on the FCEV due to their lower cost, with adequate performance and efficiency. For comparison, the Honda FCX Clarity has a rated range of 620 km (387 miles) with a 35 MPa H_2 cylinder, while the Toyota FCV has a rated range of 830 km (516 miles) with a 72 MPa H_2 cylinder, without refueling, in the standard Japanese 10–15 mode drive-cycle test. While the latter numbers are certainly impressive, fuel cell researchers must expect a continuing race.

It may seem strange to focus on these very practical aspects in a somewhat fundamental review, but the fact is that they drive our efforts forward. Thus, the push to decrease platinum loadings in the fuel cell cathode while retaining high performance has never been stronger than at the present time. With this in mind, we review some of the more promising recent developments along these lines around the world, as well as some of our own efforts.

While it would be highly desirable to totally eliminate platinum and/or platinum group metals (PGM), the performance thus far, at least in the proton-conducting membrane-type fuel cell, has not been adequate. It has been concluded that we must rely on PGMs in the near term but greatly decrease the loadings. In principle, there are two main approaches: (a) increase the actual intrinsic catalytic activity and (b) increase the utilization and effectiveness of either pure platinum or that of a well-known alloy such as Pt_3Co. Of course, both of these approaches are interrelated and often difficult to separate. Indeed, if one can accomplish both objectives simultaneously, so much the better. Probably the best example of this is the single monolayer of platinum on a less noble metal core, with increased catalytic activity. We shall describe efforts such as this later in this review.

2. Historical background

As reviewed in an earlier publication [3], platinum alloy catalysts for the ORR were developed initially by Landsman, and Luczak at United Technologies (later, International Fuel Cells) starting in the mid-1970s [4–6]. They examined the Pt–Co system and several others, including ternary alloys, for the phosphoric acid fuel cell. It was soon realized that such alloys could also be useful in PEFCs. In early scientific studies, it was proposed that the apparent high ORR activity was simply apparent, due only to a higher surface area [7,8]. Later, several groups proposed alternate explanations based on geometric and/or electronic effects, as we will describe next.

Following the lead of Landsman and Luczak, one of the present authors (MW) worked on Pt–Co and other alloys in the early 1990s in collaboration with researchers at Tanaka Precious Metals and Stonehart Associates [3,9]. Even at this time, ternary and even quaternary alloys were considered, for example, Pt–Co–Ni and Pt–Fe–Co–Ni [9]. In the 1994 article, the idea of the platinum "skin" layer was mentioned, which forms via redeposition of Pt dissolved from small particles onto larger alloy particles in hot phosphoric acid [3]. At this early stage, there was already a discussion of competing ideas to explain the enhanced activity. Gottesfeld and coworkers had proposed a simple surface area effect [7,8]. Beard and Ross proposed the formation or enhancement of a Pt(100)-like surface, with an enhancement in catalytic activity [10]. Jalan and Taylor proposed an optimal interatomic spacing, which would enhance the splitting of the O_2 molecule [11]. This idea has continued to enjoy a wide following, as discussed later, due to its reasonableness. However, the authors also pointed out the possibility that other important properties might also track the interatomic spacing.

However, in the early paper from the University of Yamanashi, arguments were given first that a surface area effect would not be able to explain the results, due to a "renewal" of the surface, such that roughness would be removed, and also the catalytic effect was observed irrespective of the extent of corrosion, which was quite different for ordered vs. disordered alloy particles [3]. It was also argued that a specific type of surface structure was also unlikely, also due to the renewal of the surface. The authors instead argued for an electronic effect: "the catalytic enhancement might be attributed to a modification of an electronic structure or a chemical property of Pt by additional elements, affecting a charge transfer or a reactant adsorption in the process of O_2 electroreduction." Nearly 20 years later, there is still merit in this statement, and substantial evidence has been obtained in support of it, but it still remains controversial.

Several years later, the topic of platinum alloys was again taken up in the senior author's laboratory, in a series of articles, starting in 1998, on Pt–Ni alloy sputtered films [12–14]. In the first paper in this series, ORR enhancement factors up to approximately 10 were found, with no dependence upon roughness. All of the alloys were found to become completely covered by an "extremely thin" "Pt skin layer." Based on the x-ray photoelectron spectroscopic results, this layer was estimated to be less than 1 nm thick [12]. The XPS spectra exhibited core level shifts relative to the pure metals: in $Pt_{80}Ni_{20}$, the Pt $4d_{3/2}$ and Pt $4d_{5/2}$ peaks were shifted to higher binding energy, while the Ni $2p_{1/2}$ and Ni $2p_{3/2}$ peaks were shifted to lower binding energy. It was argued that this was evidence of an electronic effect. It was also argued that the interatomic distance (Pt–Pt) should not be perturbed significantly due to the skin layer being pure Pt. As discussed later, this idea is very difficult to check experimentally, but it is quite likely that small changes do exist even on the pure Pt skin. Both of these points were controversial at that time and in fact still remain controversial, but we will discuss them further in the light of the results accumulated during the past 14 years. Regarding the specific reason for the enhancement, it was proposed that the modified electronic properties of the Pt skin with underlying Pt–Ni alloy led to an increase of the electronic charge transferred to the adsorbing oxygen molecule, increasing the adsorption energy and lengthening the O—O bond, facilitating the dissociation. However, since the Tafel slope was unchanged, there was thought to be no change in the ORR mechanism itself.

In the second paper in this series, various alloys in the Pt–Fe system were examined in the form of sputtered films [14]. A maximum in the ORR activity was found for ca. 50 atomic % Fe, for which an enhancement factor of ca. 20 was found, which was not dependent upon roughness. We should note that later estimates of the enhancement factors were lower, however. Again, after exposure to acid solution, all of the films were found to be pure Pt at the surface. The XPS spectra again showed an increase in binding energy

for the Pt $4d_{3/2}$ and $4d_{5/2}$ peaks for the alloys, but, in contrast to Ni, also an increase in binding energy for Fe 2 $p_{1/2}$ and $2p_{3/2}$. As with the previous paper, the shift in the Pt levels was seen as evidence for a lowering of the Fermi level and therefore, a decrease in the d-band occupancy (increase in the number of d-band vacancies), in agreement with the XAS study of Mukerjee et al. [15]. However, this idea was modified in a later paper, as discussed below. It was also pointed out that the magnitude of the binding energy shift decreased after exposure to the electrolyte, due to the formation of the pure Pt surface layer. Also as in the previous paper, it was argued that a possible reason that some workers had not observed a binding energy shift was that perhaps the surface Pt film may have been too thick.

In the third paper in this series, Pt–Fe, Pt–Co and Pt–Ni films were compared [13]. It was shown that the Pt–Fe alloys were the most active, followed by Pt–Co and then by Pt–Ni. In the XPS results, all of the alloys exhibited positive binding energy shifts for the Pt $4d_{3/2}$ and $4d_{5/2}$ peaks. Interestingly, the positive shifts for the $2p_{1/2}$ and $2p_{3/2}$ peaks followed roughly the same trends as for the ORR activity, i.e., Fe > Co > Ni. Again, as in the previous two papers, it was argued that the increase in ORR activity was due to the transfer of electronic charge to the adsorbed O_2 to an extent larger than that with pure Pt, therefore, with an additional lengthening of the O—O bond. As we will discuss further, this effect might not be due to an increase in d-band vacancies but rather a decrease, i.e., raising of the Fermi level. Nonetheless, the basic idea of electronic charge being transferred from the metal surface into antibonding π orbitals of O_2 still seems to be a very reasonable hypothesis, even if the details remain to be worked out. Thus, we can see that these early papers essentially laid a kind of foundation for later work.

Subsequently, an in situ scanning tunneling microscopic (STM) study was carried out in our laboratory [16]; in this work, it was found by direct observation that a pure Pt skin layer was formed on a Pt–Fe sputtered alloy film after potential cycling in 0.1 M $HClO_4$ solution at ambient temperature. After 10 cycles between 0.05 and 0.95 V vs. RHE, Pt(111) terraces were observed to have formed (Fig. 1). The interatomic distances were measured directly and found to be 0.28 nm ± 0.02 nm, close to that for pure bulk Pt. A similar skin layer formation was observed also on a Pt–Co sputtered alloy film.

In a follow-up study with the electrochemical quartz crystal microbalance (EQCM) technique, essentially the same phenomenon was observed, with both Fe and Pt being dissolved and Pt being redeposited to form a pure Pt skin layer [17]. The dissolution of Fe, as well as Co, was monitored with the EQCM in terms of mass, with simultaneous measurement of the cyclic voltammetric behavior, which showed a convergence to that of pure Pt (Fig. 2). This paper also summarizes the results from several other papers from this laboratory on the subject of CO-tolerant hydrogen oxidation reaction (HOR) activity of Pt–Fe, Pt–Co and Pt–Ni alloys. It was found in that work that the Pt skin layer possessed altered properties for CO adsorption, as evidenced by the stripping peak potential as well as changes in C–O vibrational frequencies and also decreases in CO coverage, which were indicative of weakened adsorption energy [18]. This modified behavior was also ascribed to an increased level of d-band vacancies, but again, this hypothesis was reinterpreted in later work, as described below. The main point is that the electronic properties of the Pt skin layer were indeed modified. In this case, the Pt–Pt distance would play a lesser role, due to the atop nature of the CO adsorbed species that was examined in the infrared spectra. In addition, the HOR behavior itself was considered to be nearly unmodified, with the main difference in behavior being due to the decreased CO coverage.

In a paper from this laboratory devoted to the temperature dependence of the ORR on Pt and its alloys, it was reported that the apparent rate constants for the ORR were a factor of 2.4–4.0 higher than that on pure Pt, i.e., somewhat lower enhancement factors than those obtained earlier, while the activation energies were essentially unchanged compared to pure Pt, with a value of 41 kJ mol^{-1} at a potential of −0.525 V vs. the reversible potential

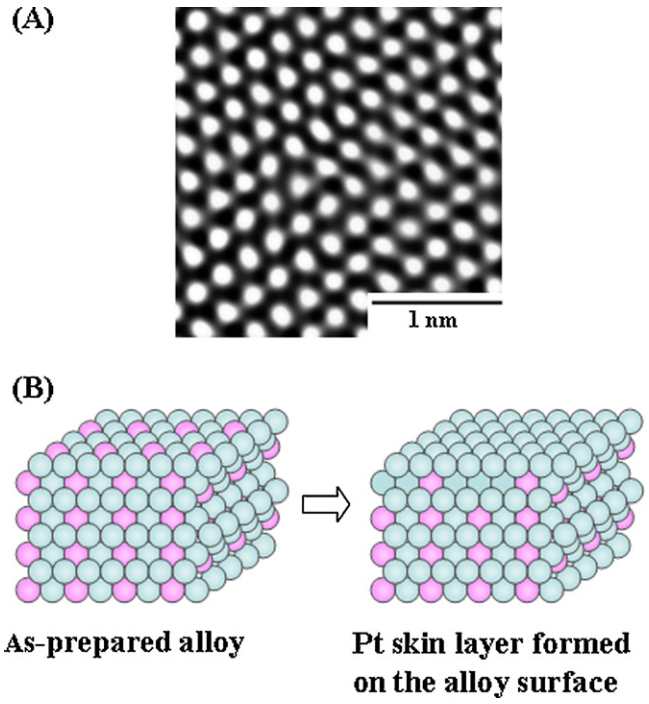

Fig. 1. (A) Atomic resolution STM image (3 nm × 3 nm) of a Pt skin layer formed on $Pt_{64}Fe_{36}$ alloy after the EC-stabilization. The image was observed at 0.5 V in 0.1 M $HClO_4$ (from Ref. [16], reproduced with permission of The Royal Society of Chemistry). (B) Schematic diagram of the Pt skin layer on the Pt alloy.
(from Ref. [26], reproduced with permission of The Electrochemical Society of Japan.)

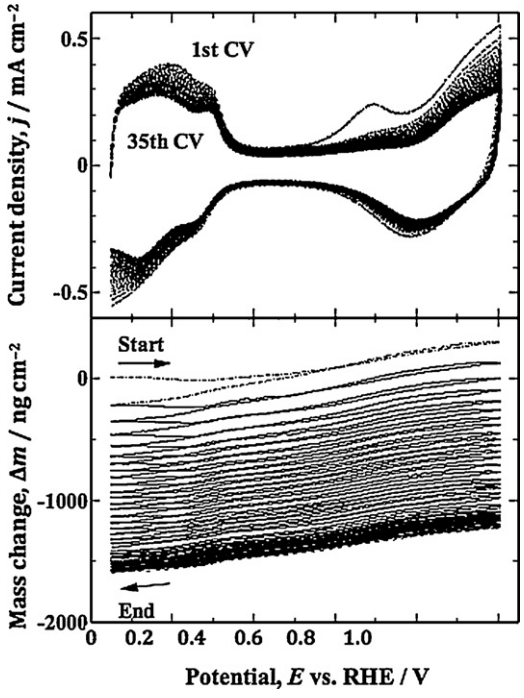

Fig. 2. (A) Cyclic voltammograms and (B) simultaneous mass changes during repetitive potential sweeps at a $Pt_{65}Fe_{35}$ alloy EQCM electrode in 0.1 M $HClO_4$ at 25 °C; potential sweep rate, 20 mV s^{-1}.
(from Ref. [17], by permission of Elsevier, Ltd.)

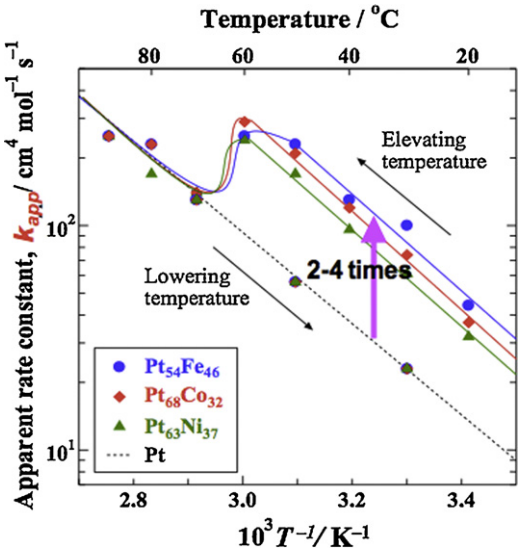

Fig. 3. Arrhenius plots of k_{app} for the ORR at (●) $Pt_{54}Fe_{46}$, (♦) $Pt_{68}Co_{32}$, (▲) $Pt_{63}Ni_{37}$ and (···) Pt electrodes in 0.1 M $HClO_4$ at −0.525 V vs. E^0.
(from Ref. [19], by permission of The American Chemical Society.)

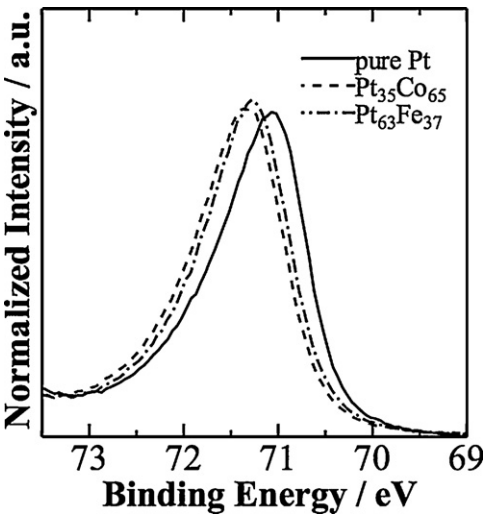

Fig. 4. Area-normalized core-level (CL) spectra of Pt4f$_{7/2}$ for pure Pt (solid line), Pt skin/$Pt_{35}Co_{65}$ (dashed line) and Pt skin/$Pt_{63}Fe_{37}$ (dash-dotted line) after the electrochemical stabilization; the emersion potential was 1.00 V vs. RHE.
(from Ref. [25], by permission of John Wiley & Sons, Inc.)

[19]. This was consistent with the Tafel slopes being similar but with the exchange current densities being increased. The latter exhibited the same trend as in the previous work, i.e., decreasing in the order Pt–Fe > Pt–Co > Pt–Ni. It was concluded that the pre-exponential factor in the rate expression is increased due to a higher coverage of adsorbed O_2. Later in this paper, we will discuss how this view compares with recent theoretical results.

During the experiments at increasing temperatures, the rate constants observed above 60 °C were markedly lower than those measured at lower temperatures, presumably due to Co dissolving out from the surface, leaving a thicker Pt surface layer. This effect was irreversible, i.e., the rate constants measured with decreasing temperature were also lower than those measured as the temperature was being raised (Fig. 3).

Going back to the point made above regarding CO adsorption as an indicator of modified electronic structure, we cite our more recent work on Pt–Co and Pt–Ru as CO-tolerant HOR catalysts [20]. In that paper, we showed a clear trend in XPS core level shift to higher binding energy, with Ru producing a larger shift compared to Co. This was also shown to be the trend in the weakening of the CO adsorption strength, i.e., with Ru producing the largest effect. Nearly the same degree of shift has also been found for Pt–Fe (Fig. 4). This situation can be presented in the form of a density of states (DOS) vs. energy diagram (Fig. 5), which shows the filling of the d-band of Pt from the higher level d-band states of the Co or Ru. Nørskov and coworkers (see [21] and references therein) proposed a correlation between the adsorption strength for adsorbates such as CO and the position of the d-band center. Based on work of Weinert and Watson [22], we proposed the core level shift as being a more convenient indicator, due to its easily and precisely measured position, compared to the d-band center. It should also be noted here, however, that this correlation may work in opposite directions for CO and O_2, as discussed later.

3. Recent work

In more recent work on ORR electrocatalysis, we have been focusing not only on Pt alloys but also on platinum itself, in order to understand the catalysis at the fundamental level. We have been using the combined electrochemical cell plus x-ray photoelectron spectroscopy (EC-XPS) technique to better understand well-defined surfaces of both alloys and pure platinum, particularly with single crystals, and have also been continuing to use the EQCM, or as it is more properly called now, the electrochemical quartz crystal nanobalance (EQCN).

3.1. EC-XPS studies

The EC-XPS technique has been used extensively in our laboratory to examine well-defined metal electrode surfaces [20,23–26]. It has been particularly useful in improving the understanding of the nature of the metal surface during the ORR. It has been used to study both platinum alloys in the form of sputtered films [23–25] and pure platinum single crystals [25,27,28]. Recently, we have also been able to prepare high-quality single crystals of Pt–Co alloys and will report EC-XPS results in the near future [29].

The combination of electrochemistry and high vacuum, surface science techniques such as XPS has been developed over the past nearly 40 years in various laboratories around the world, including work of Armstrong, Hansen, Hubbard, Ross, Sass, Sherwood,

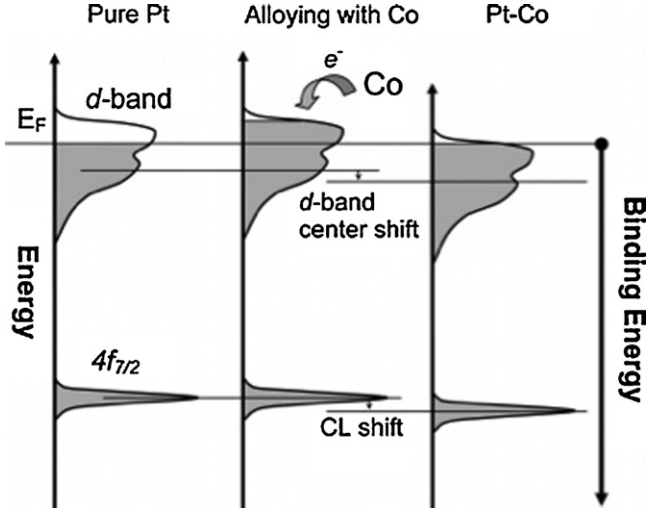

Fig. 5. Schematic explanation of the alloying effect on the electronic structures of Pt. In XPS measurement, the binding energy should be referred to E_F.
(from Ref. [20], by permission of The American Chemical Society.)

Winograd, and Yeager, to name just a few of the early workers, and also many others in later years (see review of Soriaga [30]). Our particular design is based on one developed by the Itaya group [31]. One of first to use the emersion technique was Hansen [32], in which the electrode is withdrawn from the electrolyte under potential control, with the double layer intact. This is also a key point in the EC-XPS apparatus constructed in this laboratory. Other key points are (a) that the electrode is rapidly cooled due to evaporation of the protective water droplet, so that the structure of the adsorbed layer of oxygenated species is largely preserved, including a water bilayer, and (b) the electrolyte used is HF, which is completely removed from the surface during evacuation, leaving behind no oxygen-containing anion. In the case of the alloy films, a Pt skin was preformed by potential cycling. The experimental details have been given in our previous papers.

XPS intrinsically has high surface sensitivity and high energy resolution, making it possible to resolve small differences in chemical properties, for example, redox state. This makes it possible to resolve binding energy (BE) differences between adsorbed oxygen atoms (O_{ad}), hydroxyls (OH_{ad}) and two different types of water molecules (H_2O_{ad}), which we have assigned to first and second layers. We found these same types of species on all of the different types of platinum electrodes that we examined, including polycrystalline, single crystal and alloy films. Surprisingly, the binding energies for each species were nearly constant, with negligible dependence on the type of platinum electrode, and variations within ±0.2 eV [23–25,27].

First, we will discuss results for the pure Pt single crystal surfaces, which were reported for Pt(111) [27] and then recently to compare all three low-index surfaces [28]. We compare the electrochemical behavior for Pt(111), Pt(100) and Pt(110) in Fig. 6. The differences in the hydrogen adsorption–desorption region have been well documented in many papers. However, it is interesting that the total charge for the hydrogen desorption on Pt(100) (238 μC cm^{-2}) exceeds the theoretical single monolayer coverage (208 μC cm^{-2}), as already pointed out by other groups [33,34], so that some of this charge must be due to another process. The XPS results can actually help to explain this (see below). The differences in the potential range above 0.5 V have been less well understood. The O 1s spectra for all three surfaces are shown in Fig. 7 as a function of potential. Certainly, the Pt(111) surface is unique, due to the presence of the butterfly feature, which shows up clearly in the early onset of the OH_{ad} feature (Fig. 7a).

In Fig. 7a, we can see the O 1s spectra obtained after emersion of a Pt(111) electrode at various potentials [27]. Each spectrum was fitted with asymmetric Lorentzian–Gaussian peaks with a linear background (Fig. 8a). The full width at half maximum (fwhm), tail scale (TS) and Gaussian-to-Lorentzian ratio (G/L) were maintained constant [35], and the BE peak positions were allowed to vary. Details can be found in previous papers [23,27,28]. The 529.6 and 530.5 eV peaks were assigned to OH_{ad} and O_{ad}, consistent with the assignments of Kinne et al. [36]. The 532.6 eV peak was assigned to H_2O_{ad}, consistent with that of Henderson [37]. The 531.1 eV peak was assigned to a second type of H_2O_{ad}. Based on previous studies that have studied the water bilayer on Pt(111) [37], including that of Ogasawara et al. [38], who proposed that the water layer immediately next to the Pt surface should have a lower BE O 1s peak, due to direct adsorption in the atop configuration of the oxygen atom to a Pt atom. Thus, we assign the 531.1 eV peak to this first layer water, $H_2O_{ad,1}$, and the 532.6 eV peak to the second layer water, $H_2O_{ad,2}$, which is hydrogen-bonded to the first layer. The spectral intensities for the $H_2O_{ad,2}$ species were usually somewhat lower than those for $H_2O_{ad,1}$, probably due to partial desorption of this more weakly bound species. The potential dependences of these species were found to reasonably correspond to the initial oxidation of water at potentials above 0.6 V vs. the reversible hydrogen electrode (RHE):

$$H_2O_{ad} \rightarrow OH_{ad} + H^+ + e^- \quad (1)$$

and the subsequent oxidation of OH_{ad} at potentials above 0.9 V vs. RHE:

$$OH_{ad} \rightarrow O_{ad} + H^+ + e^- \quad (2)$$

so that the coverage of OH_{ad} decreased as that of O_{ad} increased. It was shown in our 2009 paper for the first time that the current peak in the cyclic voltammogram at ca. 0.6 ("butterfly region"; see Fig. 6) was due to reaction (1) [27].

In the same way, the spectra for the Pt(100) and Pt(110) single crystal surfaces were obtained, as shown in Fig. 7b and c, respectively, as a function of emersion potential. The behavior on these two surfaces was clearly different from that for the Pt(111) surface, due to the absence of a butterfly feature. The spectra for all three surfaces are shown at potentials of 0.7 and 1.0 V in Fig. 8, with the component peaks for the various oxygen species, on the basis of the fitting. There is a clear difference in the intensity at 0.7 V, again due to the OH adsorption on Pt(111) in the butterfly region. Essentially the same four species were found on all three surfaces, with the peak BEs shown as a function of potential in Fig. 9. For Pt(111), the BEs were constant within a range of ±0.09 eV. The BE values for $H_2O_{ad,1}$ for Pt(111) were slightly lower (0.15 eV) than on the other two surfaces, while the values for $H_2O_{ad,2}$ were higher (0.4 eV) than those on the other two surfaces. These differences can be explained by differences in the distances between the two layers in terms of the final state hole-screening model discussed by Ogasawara et al. [38]. The $H_2O_{ad,1}$ is thought to interact more strongly with the Pt(111) surface. The BE for O_{ad} on Pt(100) was 0.2 eV lower than on the other two surfaces, which suggests a different chemical state, e.g., adsorption conformation. This is reasonable, due to the absence of three-fold hollow sites on this surface.

The coverages for each species were determined, as outlined in more detail in the original paper [28], and are shown in Fig. 10. These varied significantly with potential and crystal face. As already mentioned, $\theta[OH_{ad}]$ began to appear on Pt(111) at potentials above 0.5 V. The $\theta[H_2O_{ad,1}]$ values also increased in this potential range due to hydrogen bonding with OH_{ad}. These two coverages became nearly equal at 0.80 V, and the sum reached a value of 0.68, which is nearly exactly consistent with that expected from a perfect water bilayer, which is shown in Fig. 11a, suggesting that the bilayer remained intact during the oxidation process (Eq. (1)), due to the stability of he hydrogen-bonded network (HBN), as shown in Fig. 11b [39,40]. At potentials above 0.90 V, $\theta[OH_{ad}]$ and $\theta[H_2O_{ad,1}]$

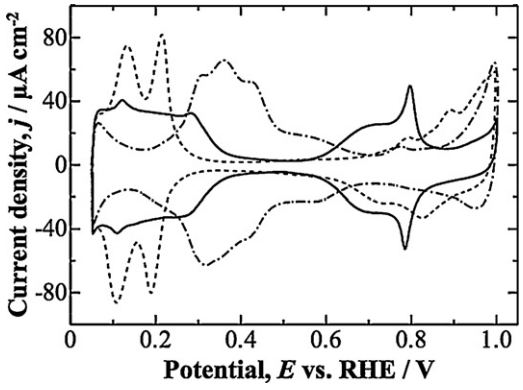

Fig. 6. Cyclic voltammograms at Pt(111), Pt(100) and Pt(110) single-crystal electrodes in 0.1 M HF solution purged with N_2 at a 50 mV s^{-1} sweep rate, indicated by solid, dash-dotted and dashed lines, respectively.
(from Ref. [28], by permission of The Royal Society of Chemistry.)

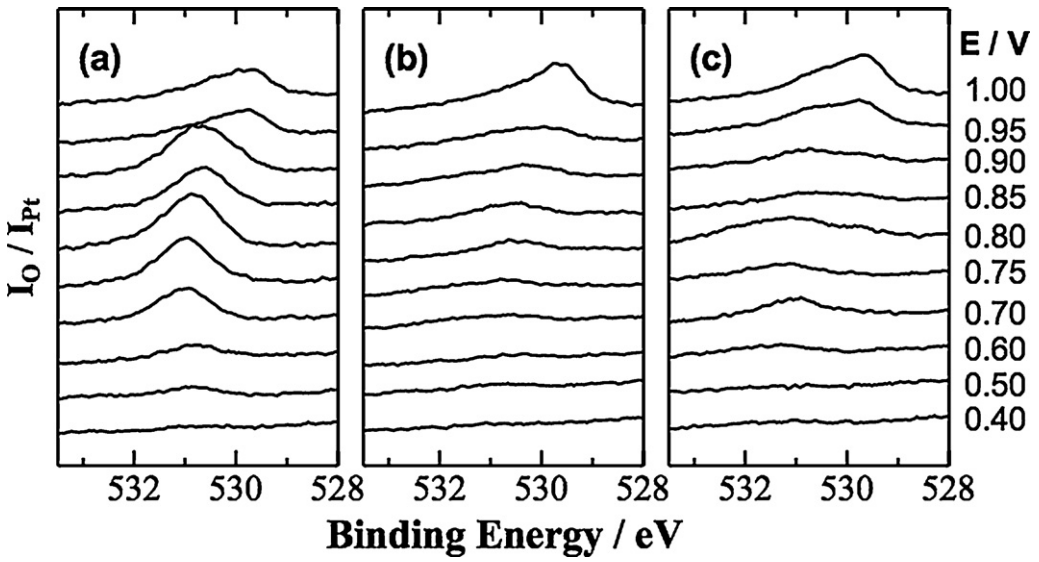

Fig. 7. Series of O 1s XP spectra for (a) Pt(111), (b) Pt(100) and (c) Pt(110) electrodes after the emersion from 0.1 M HF solution purged with N_2 at various electrode potentials from 0.4 to 1.0 V.
(from Ref. [28], by permission of The Royal Society of Chemistry.)

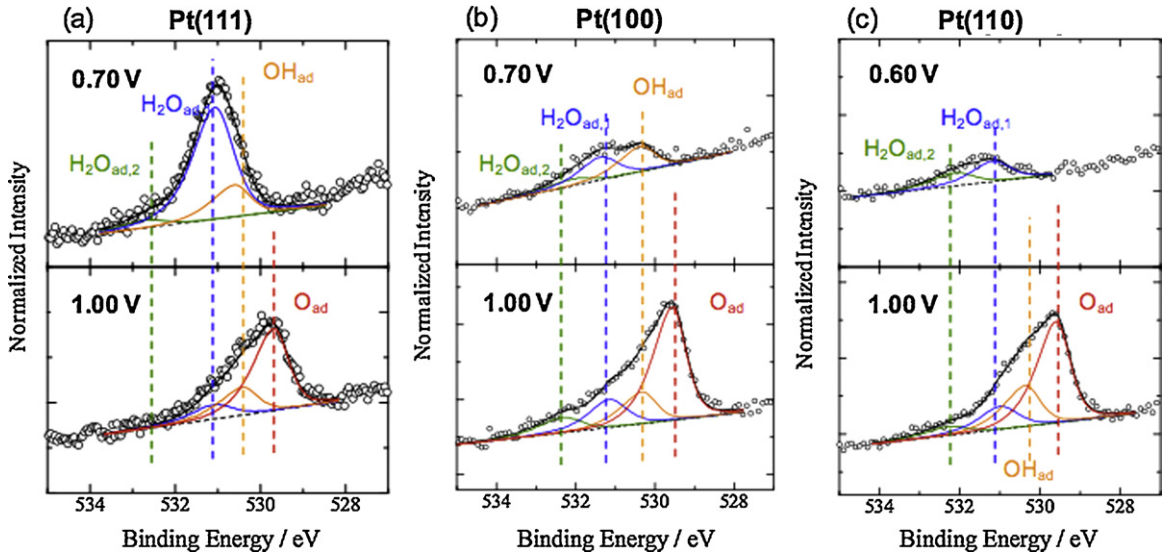

Fig. 8. Deconvolution of O 1s spectra for the three single-crystal electrodes after the emersions from 0.1 M HF solution saturated with N_2. (a) Pt(111) at 0.70 and 1.00 V. (b) Pt(100) at 0.70 and 1.00 V. (c) Pt(110) at 0.60 and 1.00 V. Open circles and colored lines indicate experimental data and the deconvoluted components, respectively. Dashed and black lines show the linear backgrounds and the resulting peaks of the composites, respectively.
(from Ref. [28], by permission of The Royal Society of Chemistry.)

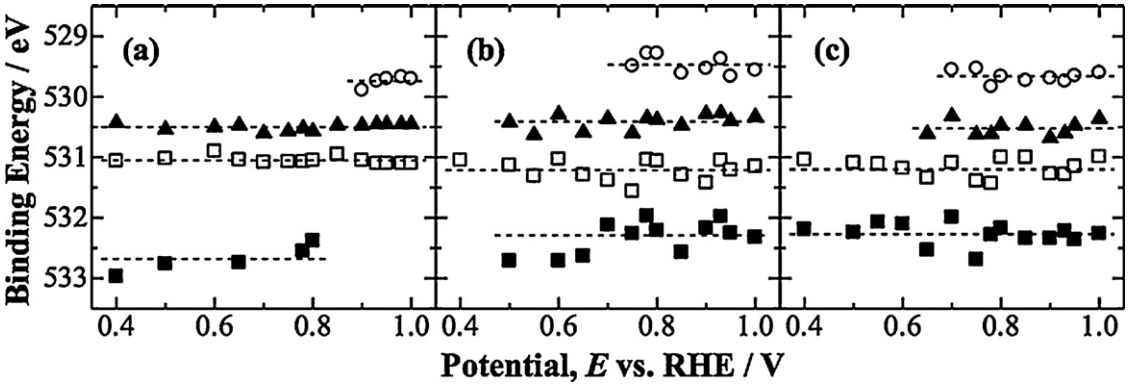

Fig. 9. Deconvoluted binding energies of O 1s for each oxygen-containing species on (a) Pt(111), (b) Pt(100) and (c) Pt(110) electrodes as a function of the electrode potential. Symbols: (■) $H_2O_{ad,2}$, (□) $H_2O_{ad,1}$, (▲) OH_{ad}, and (○) O_{ad}. Dashed lines indicate averages.
(from Ref. [28], by permission of The Royal Society of Chemistry.)

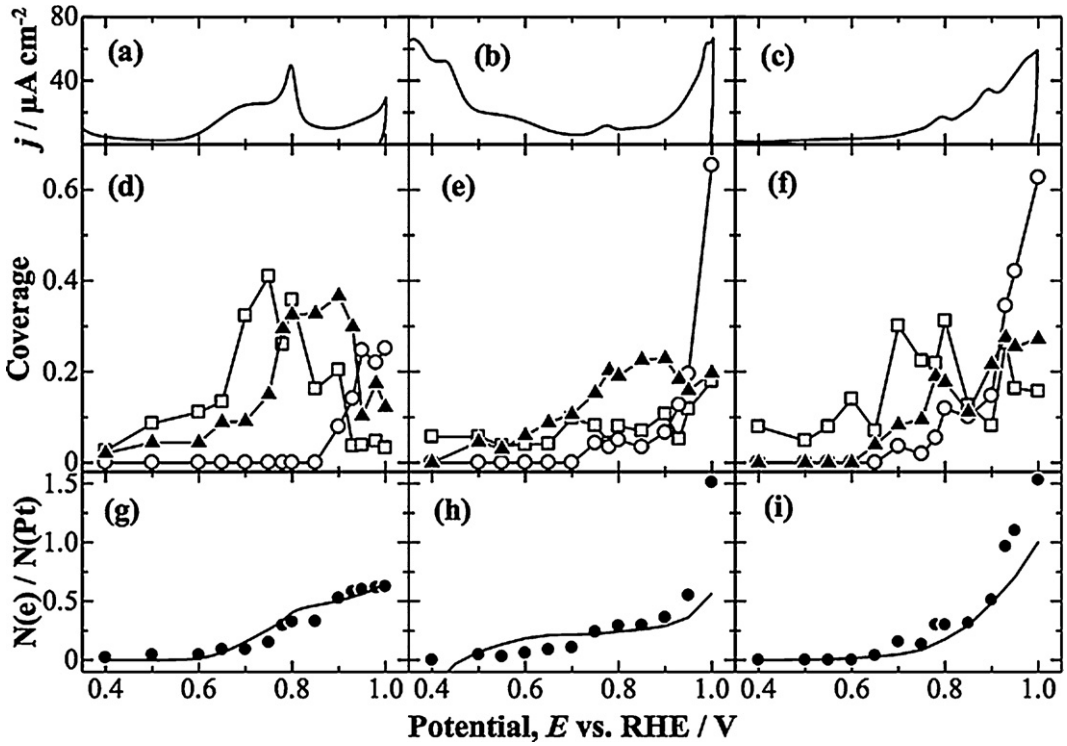

Fig. 10. Comparisons of the properties among Pt single-crystal electrodes in 0.1 M HF solution purged with N_2: voltammograms (50 mV s^{-1}) at (a) Pt(111), (b) Pt(100) and (c) Pt(110). Coverage changes of each oxygen species as a function of electrode potential at (d) Pt(111), (e) Pt(100) and (f) Pt(110). Symbols: (■) $H_2O_{ad,2}$, (□) $H_2O_{ad,1}$, (▲) OH_{ad}, and (○) O_{ad}. N(e)/N(Pt) for (g) Pt(111), (h) Pt(100) and (i) Pt(110). Solid circles and lines indicate plots based on the CV and XPS results, respectively.
(from Ref. [28], by permission of The Royal Society of Chemistry.)

both decreased, while $\theta[O_{ad}]$ increased, due to the oxidation of OH_{ad} (Eq. (2)).

As described in the original papers, the numbers of electrons transferred during these two reactions were calculated both from the integrated XPS intensities and from the cyclic voltammograms [23,27,28]. These values are shown in Fig. 10(g), (h) and (i) in terms of the number of electrons per Pt atom, e/Pt. For each surface, these values were quite consistent with each other, lending support to the XPS component analysis as a whole.

As already mentioned, the total integrated charge for the anodic current on the Pt(100) surface exceeded that for a monolayer of adsorbed hydrogen. The XPS analysis was able to explain this, because Fig. 10(h) shows that $\theta[OH_{ad}]$ increased above 0.5 V, accompanying the current flowing in the 0.5–0.7 region. This was reported for the first time in our previous paper [28]. That paper also explained the fact that the $\theta[H_2O_{ad,1}]$ values failed to increase in this region, and the e/Pt values calculated from the XPS were lower than expected, on the basis of the instability of the HBN on this surface, as shown in Fig. 11(c).

The earlier paper suggested that on Pt(100), it is possible for water to be oxidized directly to O_{ad} in a two-electron process:

$$H_2O \rightarrow O_{ad} + 2H^+ + 2e^- \quad (3)$$

This would help to explain the slightly higher $(e/Pt)_{XPS}$ values [28]. Based on these results, it was concluded that O_{ad} has a higher stability on Pt(111) compared to Pt(100), in agreement with calculations of Gu and Balbuena [41].

On Pt(110), $\theta[OH_{ad}]$ started to increase at 0.65 V, while $\theta[O_{ad}]$ started to increase at 0.70 V. The OH_{ad} formation accompanied the anodic features at 0.79 V and 0.89 V in the voltammogram. The $\theta[H_2O_{ad,1}]$ values also increased along with $\theta[OH_{ad}]$, probably due to the stability of the HBN, which is thought to form on this surface

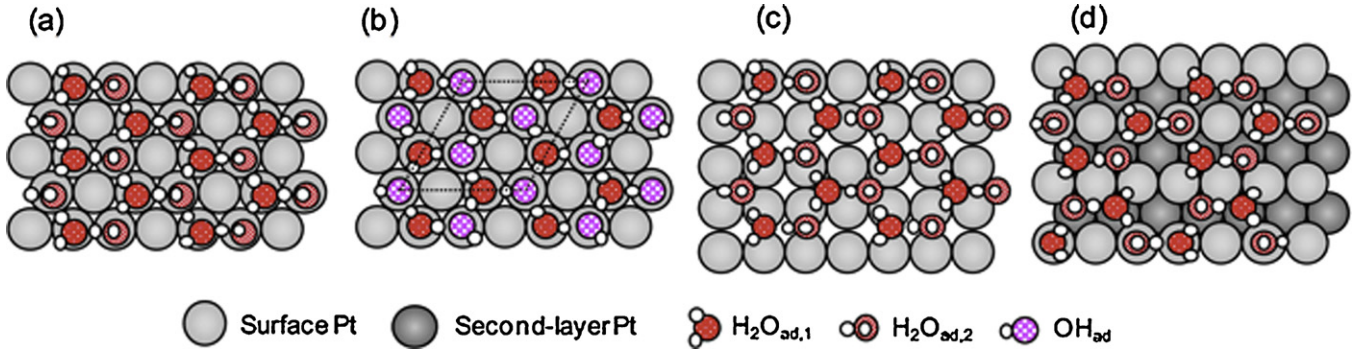

Fig. 11. Proposed structural models for (a) the bilayer water on Pt(111), (b) the mixed $OH_{ad}/H_2O_{ad,1}$ layer with the strong hydrogen-bonding network on Pt(111), (c) a unstable, incommensurate water bilayer on Pt(100), and (d) a commensurate water bilayer on Pt(110).
(from Ref. [28], by permission of The Royal Society of Chemistry.)

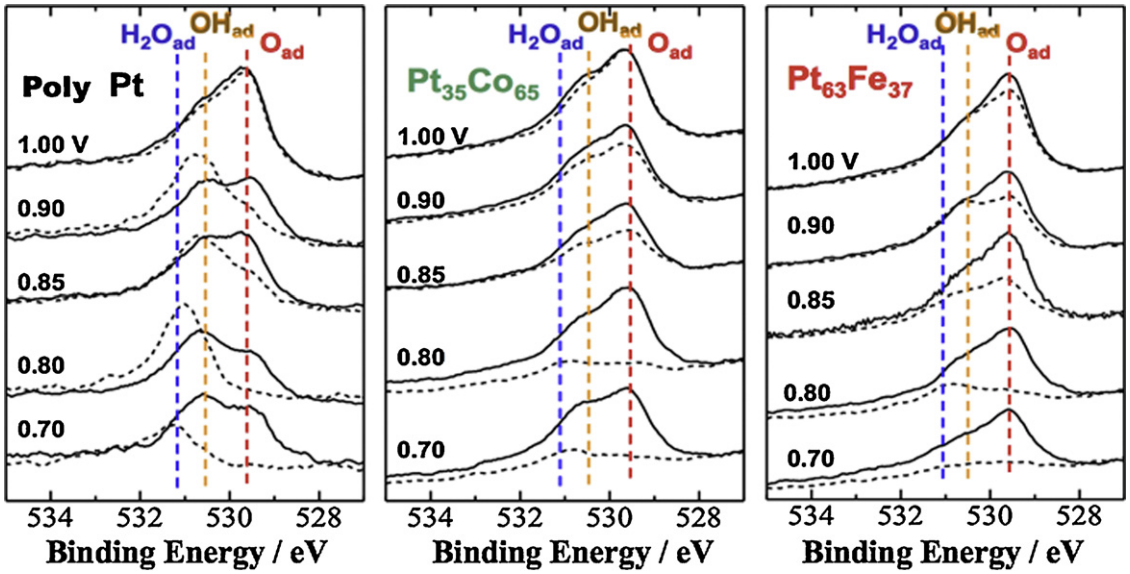

Fig. 12. O 1s spectra for poly Pt and Pt-based alloys in the electrolyte saturated with O_2 (solid line) and N_2 (dashed line). (from Ref. [24], by permission of The Electrochemical Society.)

[42], as shown in Fig. 11(d). As previously reported, the higher $(e/Pt)_{XPS}$ values compared to $(e/Pt)_{CV}$ also indicated the probable occurrence of the two-electron oxidation of water (Eq. (3)).

Thus, these results have led to an increased understanding of the electrochemical processes occurring on Pt single crystal surfaces in the absence of an adsorbing anion such as sulfate. It should be noted that there is no evidence in these results that suggests that OH_{ad} builds up on the surface and acts as a blocking agent for the adsorption of O_2, as commonly thought (see Xu et al. [43] and Roques et al. [44] and references therein). There is virtually no correlation between the potential dependences of $\theta[OH_{ad}]$ on the various surfaces and the accepted ORR activities, which decrease in the order Pt(110) > Pt(111) > Pt(100). For example, the $\theta[OH_{ad}]$ values for both Pt(110) and Pt(100) are rather similar. It should also be noted here, as we will report in the near future, that the behavior of these surfaces depends greatly on the presence or absence of molecular oxygen. This is similar to the situation for the Pt skin layers, as we will discuss next.

With this background, we can now return to discuss the Pt alloys again in terms of EC-XPS. In this case, we can illustrate the effect of the presence of an O_2 atmosphere. The O 1s XPS spectra for sputtered films of pure Pt, $Pt_{35}Co_{65}$ and $Pt_{63}Fe_{37}$ are shown as a function of potential in Fig. 12(a)–(c). Again, these alloy films were preconditioned by potential cycling in order to produce a pure Pt skin layer. Significant effects are seen for the spectra obtained after the electrodes were emersed from solutions saturated with oxygen compared to nitrogen [24]. The binding energies of the respective species, $H_2O_{ad,1}$, OH_{ad} and O_{ad}, were all very close to those observed for the single crystal Pt electrodes already discussed above, demonstrating the relative insensitivity to the type of Pt electrode. On the other hand, the coverages were highly dependent on the metal surface.

In these measurements with HF electrolyte, the ORR activities were also higher for both alloys compared to pure Pt, as already reported for $HClO_4$ electrolyte (Fig. 3) [19]. These results are shown as linear sweep voltammograms in Fig. 13(a), with Pt–Fe showing the highest activity, followed by Pt–Co and then pure Pt. After the electrodes were exposed to nitrogen atmosphere during the electrochemical potential holding step, there were noticeable changes in coverages of O_{ad} (Fig. 13b, increase) and $H_2O_{ad,1}$ (Fig. 13d, decrease) for the two alloy films compared to pure Pt. With oxygen

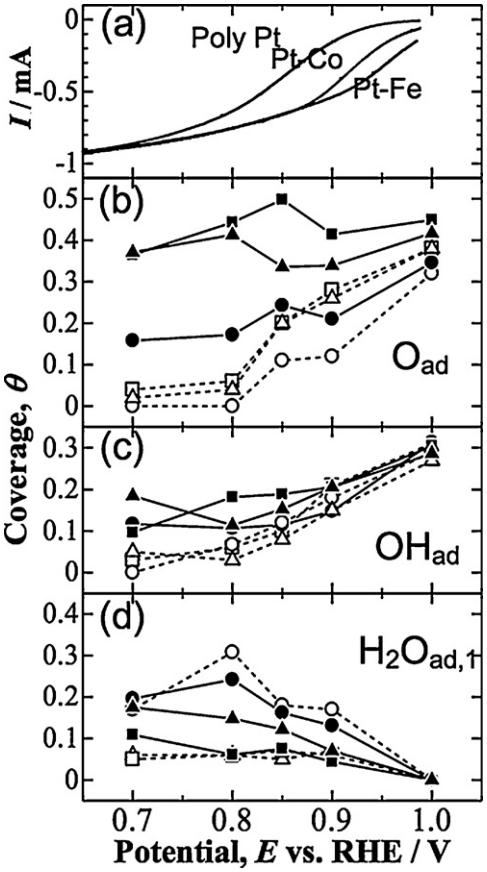

Fig. 13. (a) Linear-sweep (2 mV s^{-1}, negative-going) voltammograms for ORR at pure Pt, Pt skin/$Pt_{40}Co_{60}$ and Pt skin/$Pt_{63}Fe_{37}$ electrodes in O_2-saturated 0.1 M HF solution. Coverage of oxygen species, (b) O_{ad}, (c) OH_{ad}, and (d) $H_2O_{ad,1}$ on poly Pt, Pt skin/$Pt_{40}Co_{60}$ and Pt skin/$Pt_{63}Fe_{37}$ electrodes in N_2-(dashed lines) and O_2-(solid lines) saturated solutions. Circles, triangles and squares indicate the coverages on poly Pt, Pt skin/$Pt_{40}Co_{60}$ and Pt skin/$Pt_{63}Fe_{37}$, respectively. (from Ref. [24], by permission of The Electrochemical Society.)

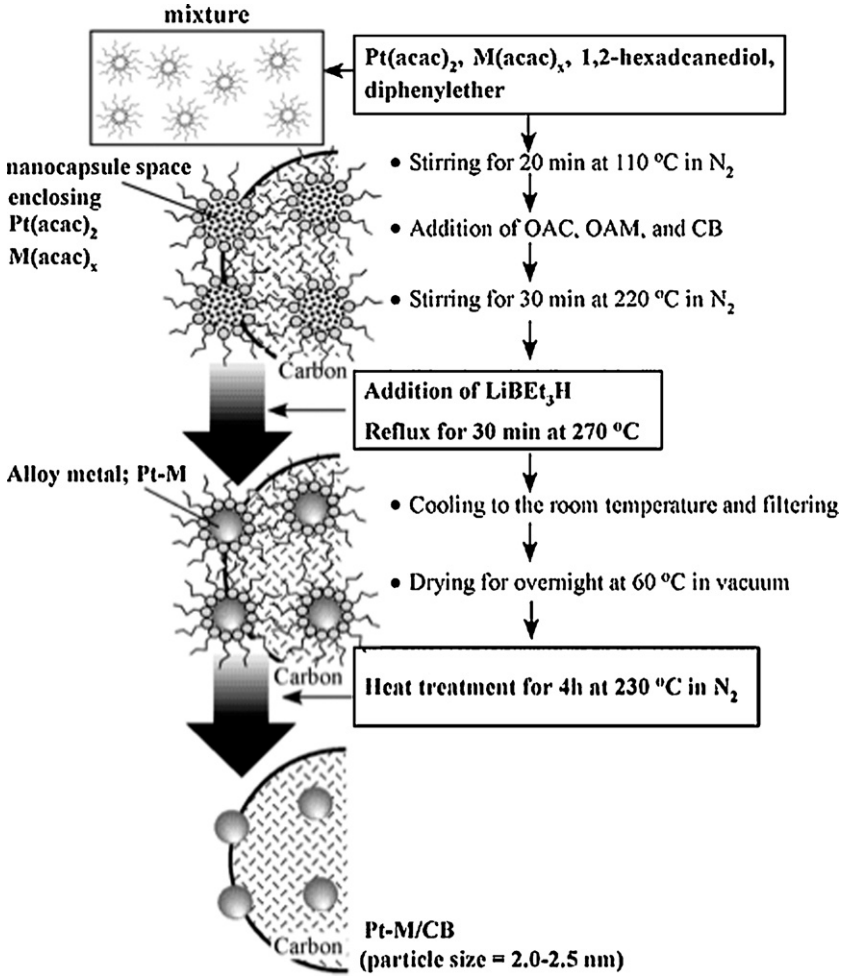

Fig. 14. Illustration of the preparation protocol for Pt/CB and Pt-M/CB catalysts.
(from Ref. [48], by permission of The American Chemical Society.)

atmosphere, however, a striking increase in $\theta[O_{ad}]$ was observed for the two alloy film electrodes. On the other hand, the $\theta[OH_{ad}]$ values increased to a smaller degree for the alloys. The $\theta[O_{ad}]$ values showed less decrease with decreasing potential for the alloys compared to pure Pt. The O_{ad} is thought to be produced via O_2 dissociation:

$$O_2 \rightarrow 2O_{ad} \quad (4)$$

Thus, it can be hypothesized that the increased ORR activity is associated with higher activity for this step.

The subsequent two steps in the ORR might be assumed to be

$$O_{ad} + H^+ + e^- \rightarrow OH_{ad} \quad (5)$$

$$OH_{ad} + H^+ + e^- \rightarrow H_2O \quad (6)$$

The second step (Eq. (5)) could be considered to be somewhat slow, due to the significant accumulation of O_{ad} and much lesser accumulation of OH_{ad}. The third step (Eq. (6)) can be assumed to also be slow, but not as slow as [5], due to the small, but non-negligible, accumulation of OH_{ad}. Here again, it should be stressed that there is no evidence of OH_{ad} acting as a site blocker, as often considered, because, in fact, $\theta[OH_{ad}]$ did increase on the alloys.

3.2. Pt electrocatalyst preparation and testing

In parallel with our efforts on the fundamental aspects of ORR electrocatalysis, we have been intensively investigating ways to put fundamental understanding into practice, through research on platinum and platinum alloy nanoparticle catalysts on various support materials. Here, we focus on recent work in which we have optimized methods to prepare monodisperse nanoparticles with a high degree of uniformity of distribution on carbon blacks (CB) and graphitized carbon blacks (GCB) [45–47], including work with Pt alloy nanoparticles [48,49].

In the early stages of development, we realized that the full catalytic power of Pt nanoparticle electrocatalysts could only be tapped if they were highly uniformly distributed on the support surface [50]. More recently, it also became apparent that uniform particle size was also advantageous. Thus, the combination of both approaches has become an important goal. Basing our approach on the proven methods developed for the preparation of absolutely monodisperse, unsupported magnetic Pt alloy nanoparticles [51–53], we adapted these methods for use with carbon black supports [48]. This approach, which is based on the use of reverse micelles or "nanocapsules," is shown diagrammatically in Fig. 14.

The resulting CB-supported material is shown in the transmission electron microscopic (TEM) images in Fig. 15, with the particle size histograms shown at the right. The latter show that the particle size distributions are quite narrow. It was found that the Pt loadings could be varied over a broad range, from 10 wt% to 55 wt%, without a significant change in the particle size (Fig. 16).

This method is well-suited for fine-tuning both the particle size, between 2.0 and 4.5 nm, and the molar ratio of metals, within a

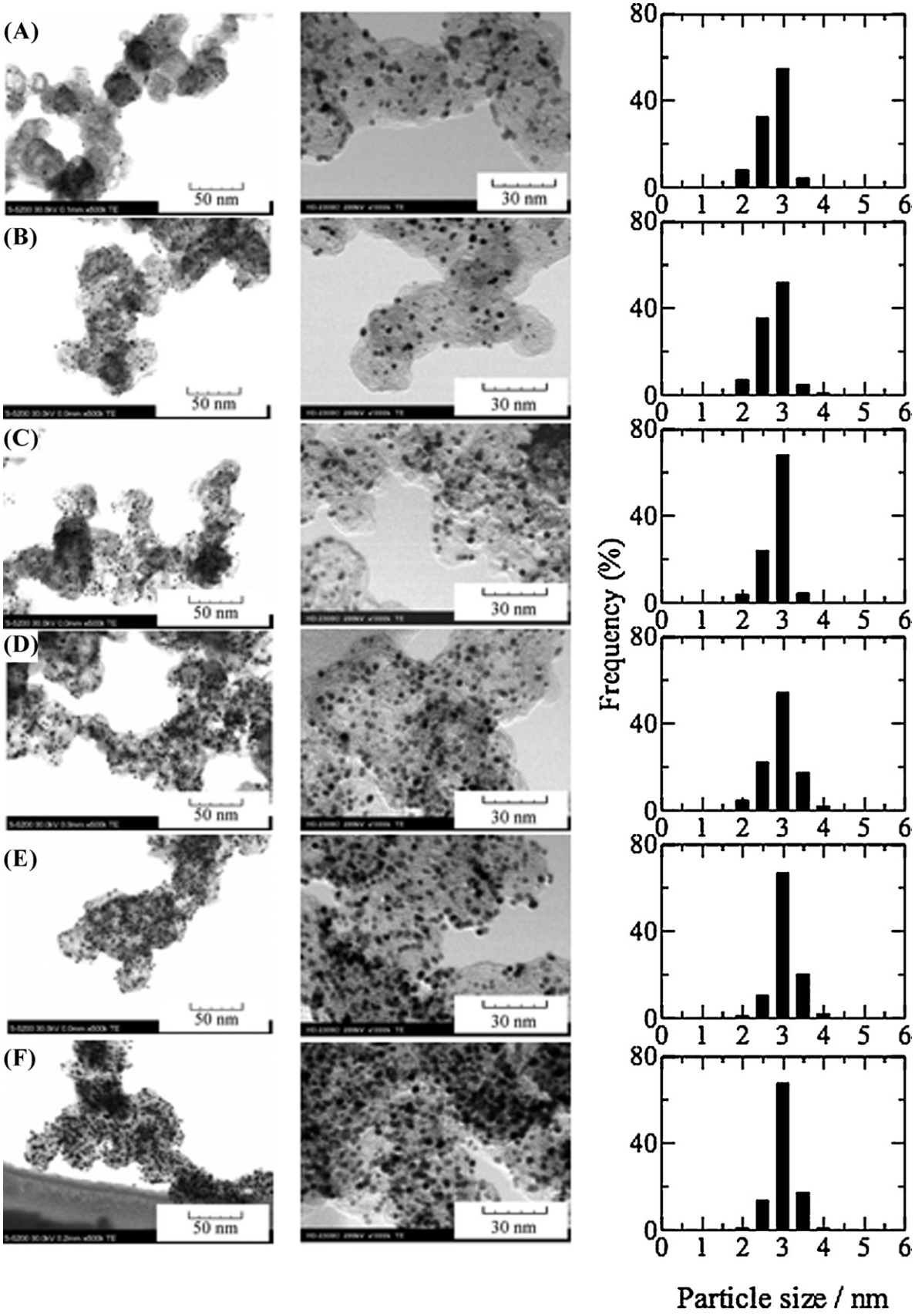

Fig. 15. STEM images (left row: low magnification, 2nd row: high magnification) and particle size distribution histograms of Pt/CB powders with various Pt loading level. (A) 10.1 wt%, (B)17.5 wt%, (C) 25.2 wt%, (D) 33.0 wt%, (E) 42.6 wt%, (F) 55.0 wt%.
(from Ref. [48], by permission of The American Chemical Society.)

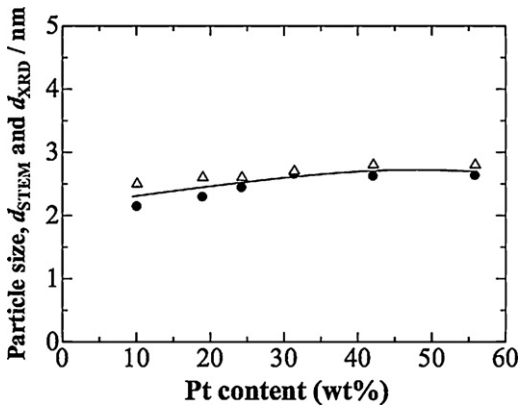

Fig. 16. Changes in the average particle sizes determined by STEM, d_{STEM}, (Δ) and the crystallite sizes determined by XRD, d_{XRD}, (●) as a function of Pt loading level on Pt/CB catalysts.
(from Ref. [48], by permission of The American Chemical Society.)

narrow range, for example, within ±1.4 at% for Pt_3Co, while still maintaining the very narrow size distribution [49].

Recently, it has become increasingly apparent that the durability of conventional CB support materials is inadequate under actual fuel cell operating conditions, and thus many research groups have been focusing on alternate support materials. It is desirable to preserve the advantages of carbon in terms of electronic conductivity and aggregate formation, and therefore, the graphitized counterpart, GCB, is attractive. However, due to the fact that the GCB particle surface is similar to that of the graphitic basal plane, it has been difficult to achieve adequately uniform distribution of the Pt nanoparticles on the surface, due to a lack of adhesion. Fortunately, with the present, nanocapsule-based approach, it has become possible to achieve highly uniform dispersions while maintaining the monodispersity [47].

With this type of Pt/GCB material, the benefits of the GCB support in terms of durability can be realized. The Fuel Cell Commercialization Conference of Japan (FCCJ) has developed protocols for accelerated durability testing of supported electrocatalysts (see [47]). The 2007 protocol involves cycling the electrode potential back and forth between 0.9 V and 1.3 V vs. RHE, with each potential being held for 30 s, each cycle lasting 60 s, in 0.1 M $HClO_4$ at

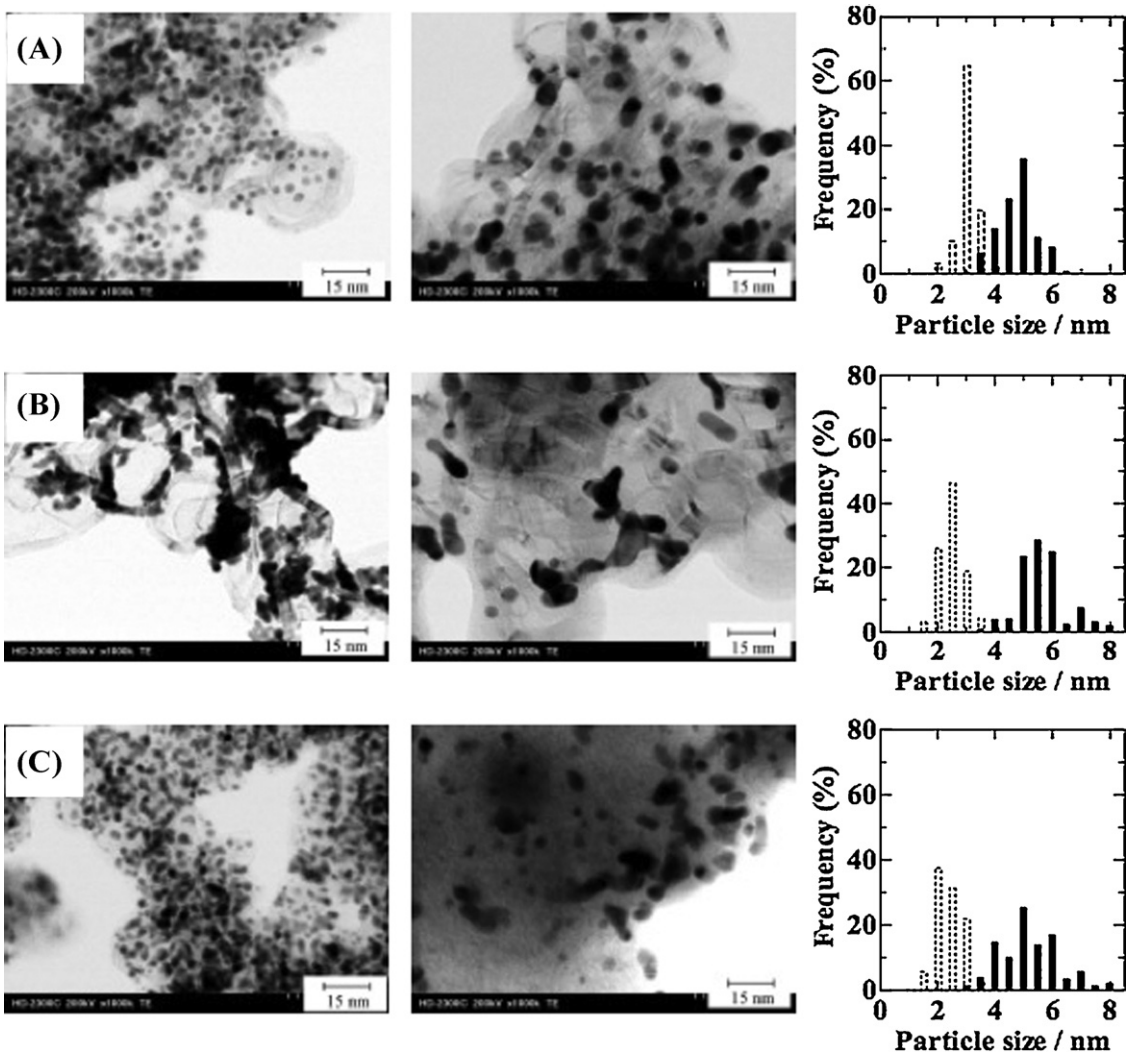

Fig. 17. STEM images (left row: low magnification, second row: high magnification) and particle size distribution histograms for 500 particles of pristine powders of (A) n-Pt/GCB, (B) c-Pt/GCB and (C) c-Pt/CB. STEM images (left row: low magnification, second row: high magnification) and particle size distribution histograms of (A) n-Pt/GCB, (B) c-Pt/GCB, and (C) c-Pt/CB powders after the durability test ($N = 5000$).
(from Ref. [47], by permission of The Royal Society of Chemistry.)

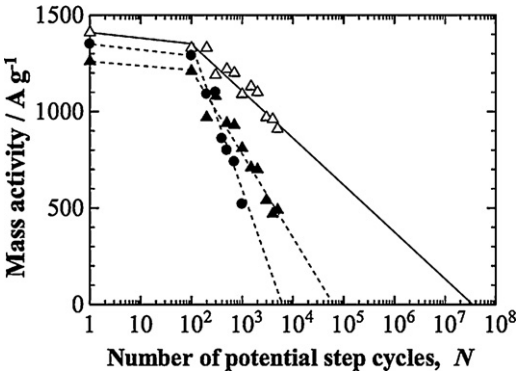

Fig. 18. Plots of mass activity (*MA*) determined at 0.80 V at Nafion-coated (△) n-Pt/GCB, (▲) c-Pt/GCB, and (●) c-Pt/CB electrodes as a function of log [*N*]. (from Ref. [47], by permission of The Royal Society of Chemistry.)

25 °C. This protocol provides a quite stringent test of durability. As shown in Fig. 17, however, the in-house-prepared Pt/GCB material survived 5000 cycles significantly better than either a commercial Pt/GCB or Pt/CB material. The particle size histograms showed only a modest growth in particle size for the in-house material.

Also, the catalytic activity for the ORR was checked with the rotating ring-disk technique periodically during the durability testing, and the mass activities (MA) at 0.80 V vs. RHE were measured, after correction for solution mass transport. These MA values are shown in Fig. 18 plotted vs. the logarithm of the number of potential step cycles *N*. After the first 100 cycles, the MA values tend to decay linearly as a function of log (*N*). The superior durability of the nanocapsule-prepared Pt/GCB is apparent in this plot. Thus, even though the commercial Pt/GCB made use of the same GCB material, the less favorable particle distribution on the surface appeared to be detrimental to its durability, as well as to the initial ORR performance at lower potentials, e.g., 0.7 V, at which mass transport plays a more important role. The effect of uniform dispersion on durability is subtle but probably involves two main contributions: (a) particles that are close together have a greater chance of bonding and forming larger particles, and (b) these particles may produce hydrogen peroxide in a highly localized manner, thus leading to significant corrosion and undercutting of the support, which then can lead to detachment of the Pt particles.

3.2.1. Recent results from other laboratories, including novel catalysts, new approaches

During the past five years, there has been a significant acceleration of the research activity in the PEFC-related electrocatalyst field. We would like to point out a small number of selected results here to give the reader an idea of the broad range of innovative ideas that are being pursued. First, we touch on some of the approaches for the preparation of novel types of monometallic and bimetallic materials, including nanoparticles.

One of the most compelling recent ideas has been the monolayer catalyst, which is basically a core-shell structure, but with a monolayer shell. This concept has been initiated principally by Adzic and coworkers, who have used it initially to produce monolayers of Pt on Ru for anodic fuel cell reactions such as CO-tolerant HOR as well as the methanol oxidation reaction (MOR) [54–56]. Later, they began to apply this concept for ORR catalysis [57–62]. Most recently, they have been investigating a novel type of structure in which the core is formed from a non-Pt bimetallic alloy, while the monolayer shell is still Pt [62–66]. This approach is particularly attractive, because it promises to provide enhanced durability. Most recently, these workers have developed a very interesting nanowire material, which may provide additional benefits compared to nanparticles, in terms of three-dimensional structure and electronic conduction paths [67].

In an effort to avoid the corrosion-susceptible carbon support, some groups have been pursuing unsupported, self-supporting and nanostructured carbon-free catalysts. One recent example utilizes Pt–M-based nanostructures [68]. The most promising candidate was found to be Pt–Ni with 55 wt% Ni.

Other interesting concepts being pursued by Markovic and coworkers include a trimetallic system based on an Au core and Pt–Fe shell, with enhanced durability [69], and core-shell structures in which the Pt shell is purposefully thickened somewhat to provide enhanced durability [70]. On the other hand, Chen et al. find that a Pt monolayer shell provides the best balance of ORR activity and durability [71]. Another example of a Pt–Fe shell, but with a Pd core, has recently been reported [72].

3.3. High throughput, combinatorial approaches

The combinatorial approach to the discovery of new and optimized compositions for electrocatalysts was pioneered by Mallouk and coworkers, initially to seek catalysts that were active for both oxygen reduction and oxygen evolution, i.e., bifunctional oxygen catalysts [73]. This approach has been continued over the last several years for the discovery of PEFC cathode catalysts. For example, the Bard group has used the scanning electrochemical microscopic (SECM) technique, which provides a direct readout of the electrochemical activity using a microelectrode that is scanned over a catalyst spot on a conductive substrate [74,75]. An interesting application of this technique was to directly interrogate Pt nanoparticles with different shapes to determine their ORR activity [76]. The only disadvantage of this technique in terms of the screening of large numbers of samples is the sequential nature of the readout.

A recent attempt to provide a parallel readout was presented by Crooks and coworkers, who used a novel bipolar cell, with the ability to optically detect the extent of the anodic reaction (Ag dissolution) [77]. Other noteworthy examples of combinatorial approaches have been presented by Guerin et al. [78,79] and by He et al. [80,81].

3.4. Computational high throughput approaches

The computational approach to combinatorial discovery is highly attractive, because in principle, there is no limit to the number of combinations and structures that can be examined, under carefully controlled conditions. Greeley and coworkers have been quite active in this area [82–84]. Froemming and Henkelman have presented a genetic algorithm that seeks to match the d-band level of Pt with a non-Pt alloy, e.g., Pd–Co [85]. However, as discussed below, we do not generally support the underlying assumptions made by these studies, i.e., that O_{ad} and OH_{ad} act to decrease the ORR activity.

3.5. Novel nanoparticle morphologies

There have been several recent exciting developments in the area of novel nanoparticle morphologies. As already mentioned above in connection with SECM, the particle morphology itself can have a significant impact on catalytic activity. The Strasser group has made extensive use of the dealloying technique to prepare core-shell structures with graded compositions [86–101]. This group has proposed that compressive strain is the main effect operating in the enhanced catalytic activity of the dealloyed nanoparticles, due to the thickness of the Pt shell, through which a ligand (electronic) effect would not be able to operate, in contrast to the much thinner Pt monolayer or skin systems, which could operate via both strain and electronic effects [94].

A new type of structure that has recently been reported is the core-dendritic shell, which has been investigated by the Crooks group [102–107]. This type of structure has the attractive feature of enhanced surface area together with unusual types of catalytic sites.

3.6. Characterization techniques

In the year following the earliest paper from our laboratory, Mukerjee et al. published in 1995 a comprehensive x-ray absorption spectroscopic (XAS) study related to the alloys of platinum with the first transition metals: Cr, Mn, Fe, Co and Ni in the form of nanoparticles supported on carbon black in a PEFC [15]. Their results showed clearly the effect of the alloying element on the electronic structure, specifically, increasing the size of the pronounced peak in the near-edge spectra for Pt (L_2 and L_3), which indicated the decreased occupancy of Pt 5d states. Their extended x-ray absorption fine structure (EXAFS) results also allowed them to obtain in situ information on the alloy nanoparticles. However, alloying is actually expected to increase the occupancy of the Pt d states, as discussed below. However, just as a brief comment at this point, the natural, simplistic assumption would be that the Pt work function would be decreased, i.e., higher Fermi level, making it in effect less noble and thus easier to oxidize. In fact, this point is also still controversial; it will also be discussed later. In any case, this is a question that still requires clarification.

X-ray absorption spectroscopy continues to be expected to provide new insights into the structural and electronic characteristics of catalysts that are important in determining both activity and stability. XAS is one of the few truly in situ techniques that are capable of doing both. The Mukerjee group continues to be active in this area [44,108], as well as the Iwasawa group [109], and the Smotkin group [110].

3.7. Theoretical studies

Surprisingly, one question that still has not been answered conclusively is whether or not there is electronic charge density transfer from a metal, such as Fe, Co or Ni to Pt. Thus, it is very interesting to see how theoretical results answer this question. There are two other associated aspects to this question, including (a) shifts of the Fermi level and (b) shifts of the d-band center. An early review of theoretical results by Rodriguez pointed out that there was no consensus in the direction of the transfer of electronic charge between the Group 10 metal (Pt, Pd, Ni) and a substrate metal, such as Ta, W or Mo, due to various problems, including the definition of the actual volume belonging to each atom [111].

Along the same lines, Xu et al. found significant shifts of the d-band centers downwards for Pt skin layers on Co for the bare surfaces but did not discuss the charge transfer in detail [43], except a brief mention that there was a slight transfer from Co to Pt.

Recently, Tang and Henkelman [112] have offered a solution to the problem of assignment of charge by suggesting a non-arbitrary method for determining the atomic volume dimensions; thus, they find that there is significant electronic charge transferred from, for example, Mo, Co and Cu to Pd, and that this charge is greater when the lowering of the d-band center is greater. These authors emphasize the simple idea that charge should always flow from a metal with a higher Fermi level (e.g., Mo, Co) to a metal with a lower Fermi level (e.g., Au, Ag, Pd). This concept is basically a semi-quantitative version of the qualitative picture that we presented for d-band filling in Fig. 5. These trends should certainly be similar for Pt. On the other hand, a study by Xin et al. compares several different ways of assigning atomic charges and therefore determining charge transfer but find negligible charge transfer for any of them [113].

As mentioned above, Xu et al. found significant shifts of the d-band centers downwards for Pt skin layers on Co for the bare surfaces [43] and found O_2 adsorption to be destabilized significantly on the Pt skin layer (−0.24 to −0.34 eV) vs. that on the pure Pt layer (−0.62 eV, uncompressed; −0.50 eV, 2% compressed). These authors proposed that the enhancement in ORR activity is due to the weaker adsorption of O atoms on the Pt skin surface, thus providing a more open surface for O_2 to adsorb. They also found higher transition state energies for O_2 dissociation for the Pt skin layers. This conclusion appears to be at odds with the conclusions we have drawn from our work.

A study by Tang and Henkelman focused on the energies of dissociated O_2, i.e., two adsorbed O atoms in hollow sites [112]. Their approach was to consider the Brønsted–Evans–Polanyi (BEP) relationship, i.e., that the activation energy for a simple chemical reaction decreases linearly as the negative reaction energy increases. As an indicator of the latter, they obtained the adsorptive binding energies of dissociated O_2 and found that these energies correlated well with both the shifts of the d-band center and the amount of charge transfer. Similarly to the work of Xu et al., they found that a core metal such as Co lowers the d-band center and destabilizes oxygen atom adsorption.

Another study also found a destabilization of adsorption of O_2 on the Pt skin layer but found that the energy barrier for O_2 dissociation was smaller, in this case, on a Pt monolayer on the Fe(001) surface [114]. Recent DFT results of Yang et al. on small Pt–Ni [115] and Pt–Cu [116] clusters are interesting, because they show essentially the same effect that was proposed by Toda et al. to explain the effect of the alloying element [13,14]. Specifically, the filling of the d-band of Pt due to charge transfer from the Ni or Cu leads to occupation of an antibonding π orbital of O_2 adsorbed in a bridging conformation, which lengthens and weakens the O—O bond. Other interesting points were (a) that O_2 did not adsorb stably in a bridging configuration on Pt(111), whereas it did on a $Pt_{12}Ni$ cluster, which would be qualitatively consistent with the proposed higher coverage of adsorbed O_2 mentioned earlier; (b) that the atop (Pauling) configuration was stabilized for the $Pt_{12}Ni$ cluster compared to that on the Pt_{13} cluster, which could explain the higher peroxide generation results found for some alloys; and (c) the diffusion barriers for the adsorbed O atom were found to be decreased on the $Pt_{12}Ni$ cluster, which would be important in the later stages of the ORR. It should be emphasized that these computational results were for a small cluster with gas-phase O_2 adsorption, without water or potential control, conditions that are clearly unrealistic, but still the conclusions are interesting and could serve as a starting point for further work.

In any case, it will be necessary to delve into the reasons for the differences in the results obtained from the various theoretical studies. In this context, it should be noted that an earlier study by Yang et al. [117], in which they used a slab model for $Pt_3Ni(111)$, their results were in agreement with those of Xu et al. [43], who also used a slab model, whereas the later results of Yang et al. utilized a small cluster and diverged from those of Xu et al. However, the simple difference of cluster vs. slab is clearly not the whole answer, because, for example, Ishikawa and coworkers have obtained consistent results for simulations of the HOR under realistic conditions (water, potential) on Pt(111) [118,119] and Pt(110) [120] surfaces with both approaches. Certainly, much more work needs to be done in the ORR area. One recent example that treated Pt(111), for example, included the effect of a hydrated proton [121].

4. Conclusions

While we have focused here on the purely catalytic aspects to a great extent, there are certainly other, associated issues that are

also important. One of these is the microscale engineering of the oxygen cathode to achieve the maximum performance and durability from any given catalyst. As we have briefly discussed in the section on practical catalysts, the distribution of catalyst on the support surface, the particle size distribution, the nature of the support material, and certainly the nature of the interface between support and catalyst, are all crucial. We have not even mentioned the ionomer, since introducing this aspect would have been unmanageable, but certainly it must also be considered in any real discussion of a practical catalyst layer. The ionomer has an obvious impact even on the events occurring on the catalyst surface.

This review has presented our own unique viewpoint in the area of platinum-based ORR electrocatalysis. There clearly remain several very basic questions that should eventually be resolved in future work. In the meantime, this area continues to be an extremely active one, full of innovation and controversy. We cherish the hope that out of this activity there will emerge new insights that will bring us closer to the dream of highly active, highly durable, low cost oxygen reduction catalysts that can be engineered to operate effectively in PEFCs.

Acknowledgments

We gratefully acknowledge support from the New Energy and Industrial Development Organization (NEDO) of Japan, through funding for the "Research on Nanotechnology for High Performance Fuel Cells" project.

References

[1] Y. Sato, Overview of Scenario, Roadmap and R&D Projects of Hydrogen and FCV in Japan, NEDO, 2010, pp. 1–22; www.hydrogen.energy.gov/pdfs/9_sato_0610.pdf.
[2] USDOE-USEPA, Fuel Cell Vehicles: Challenges, Energy Efficiency & Renewable Energy, 2012, pp. 1–2; www.fueleconomy.gov.
[3] M. Watanabe, K. Tsurumi, T. Mizukami, T. Nakamura, P. Stonehart, Journal of the Electrochemical Society 141 (1994) 2659.
[4] F.J. Luczak, D.A. Landsman, Ordered ternary fuel cell catalysts containing platinum and cobalt, US Patent 4,711,829, 1987.
[5] F.J. Luczak, D.A. Landsman, Ordered ternary fuel cell catalysts containing platinum and cobalt and method for making the catalysts, US Patent 4,677,092, 1987.
[6] F.J. Luczak, D.A. Landsman, Ternary fuel cell catalysts containing platinum, cobalt and chromium, US Patent 4,447,506, 1984.
[7] M.T. Paffett, J.G. Beery, S. Gottesfeld, Journal of the Electrochemical Society 135 (1988) 1431.
[8] K.A. Daube, M.T. Paffett, S. Gottesfeld, C.T. Campbell, Journal of Vacuum Science & Technology A – Vacuum Surfaces and Films 4 (1986) 1617.
[9] M. Watanabe, P., Stonehart, K., Tsurumi, N., Yamamoto, N., Hara, T. Nakamura, Electrocatalyst and process of preparing same, US Patent 5,189,00, 1993.
[10] B.C. Beard, J. Philip, N. Ross, Journal of the Electrochemical Society 137 (1990) 3368–3374.
[11] V. Jalan, E.J. Taylor, Journal of the Electrochemical Society 130 (1983) 2299.
[12] T. Toda, H. Igarashi, M. Watanabe, Journal of the Electrochemical Society 145 (1998) 4185.
[13] T. Toda, H. Igarashi, H. Uchida, M. Watanabe, Journal of the Electrochemical Society 146 (1999) 3750.
[14] T. Toda, H. Igarashi, M. Watanabe, Journal of Electroanalytical Chemistry 460 (1999) 258.
[15] S. Mukerjee, S. Srinivasan, M.P. Soriaga, J. McBreen, Journal of the Electrochemical Society 142 (1995) 1409.
[16] L.-J. Wan, T. Moriyama, M. Ito, H. Uchida, M. Watanabe, Chemical Communications (2002) 58.
[17] H. Uchida, H. Ozuka, M. Watanabe, Electrochimica Acta 47 (2002) 3629.
[18] M. Watanabe, Y. Zhu, H. Uchida, Journal of Physical Chemistry B 104 (2000) 1762.
[19] N. Wakabayashi, M. Takeichi, H. Uchida, M. Watanabe, Journal of Physical Chemistry B 109 (2005) 5836.
[20] M. Wakisaka, S. Mitsui, Y. Hirose, K. Kawashima, H. Uchida, M. Watanabe, Journal of Physical Chemistry B 110 (2006) 23489.
[21] J.K. Nørskov, F. Abild-Pedersen, F. Studt, T. Bligaard, Proceedings of the National Academy of Sciences of the United States of America 108 (2011) 93.
[22] M. Weinert, R.E. Watson, Physical Review B 51 (1995) 17168.
[23] M. Wakisaka, H. Suzuki, S. Mitsui, H. Uchida, M. Watanabe, Journal of Physical Chemistry C 112 (2008) 2750.
[24] M. Watanabe, M. Wakisaka, H. Yano, H. Uchida, ECS Transactions 16 (2008) 199.
[25] M. Wakisaka, M. Watanabe, H. Uchida, in: A. Wieckowski, J.K. Nørskov (Eds.), Fuel Cell Science: Theory, Fundamentals, and Biocatalysis, John Wiley & Sons, Inc., Hoboken, NJ, USA, 2010, pp. 147–168.
[26] H. Uchida, H. Yano, M. Wakisaka, M. Watanabe, Electrochemistry 79 (2011) 303.
[27] M. Wakisaka, H. Suzuki, S. Mitsui, H. Uchida, M. Watanabe, Langmuir 25 (2009) 1897.
[28] M. Wakisaka, Y. Udagawa, H. Suzuki, H. Uchida, M. Watanabe, Energy & Environmental Science 4 (2011) 1662.
[29] M. Wakisaka, Y. Hyuga, K. Abe, H. Uchida, M. Watanabe, Electrochemistry Communications 13 (2011) 317.
[30] M.P. Soriaga, Progress in Surface Science 39 (1992) 325.
[31] T. Yamada, N. Batina, K. Itaya, Journal of Physical Chemistry 99 (1995) 8817.
[32] W.N. Hansen, Surface Science 101 (1980) 109.
[33] A. Lasia, Journal of Electroanalytical Chemistry 562 (2004) 23.
[34] N. García-Aráez, V. Climent, J.M. Feliu, Electrochimica Acta 54 (2009) 966.
[35] P.R. Norton, Surface Science 47 (1975) 98.
[36] M. Kinne, T. Fuhrmann, J.F. Zhu, B. Tränkenschuh, R. Denecke, H.P. Steinrück, Langmuir 20 (2004) 1819.
[37] M.A. Henderson, Surface Science Reports 46 (2002) 1.
[38] H. Ogasawara, B. Brena, D. Nordlund, M. Nyberg, A. Pelmenschikov, L.G.M. Pettersson, A. Nilsson, Physical Review Letters 89 (2002) 276102.
[39] C. Clay, S. Haq, A. Hodgson, Physical Review Letters 92 (2004) 046102.
[40] G.S. Karlberg, F.E. Olsson, M. Persson, G. Wahnstrom, Journal of Chemical Physics 119 (2003) 4865.
[41] Z. Gu, P.B. Balbuena, Journal of Physical Chemistry C 111 (2007) 9877.
[42] J. Fusy, R. Ducros, Surface Science 237 (1990) 53.
[43] Y. Xu, A.V. Ruban, M. Mavrikakis, Journal of the American Chemical Society 126 (2004) 4717.
[44] J. Roques, A.B. Anderson, V.S. Murthi, S. Mukerjee, Journal of the Electrochemical Society 152 (2005) E193.
[45] H. Yano, J.M. Song, H. Uchida, M. Watanabe, Journal of Physical Chemistry C 112 (2008) 8372.
[46] H. Yano, T. Akiyama, H. Uchida, M. Watanabe, Energy & Environmental Science 3 (2010).
[47] H. Yano, T. Akiyama, P. Bele, H. Uchida, M. Watanabe, Physical Chemistry Chemical Physics 12 (2010) 3806.
[48] H. Yano, M. Kataoka, H. Yamashita, H. Uchida, M. Watanabe, Langmuir 23 (2007) 6438.
[49] K. Okaya, H. Yano, H. Uchida, M. Watanabe, ACS Applied Materials and Interfaces 2 (2010) 888.
[50] M. Watanabe, H. Sei, P. Stonehart, Journal of Electroanalytical Chemistry 261 (1989) 375.
[51] S. Sun, C.B. Murray, D. Weller, L. Folks, A. Moser, Science 287 (2000) 1989.
[52] S. Sun, S. Anders, T. Thomson, J.E.E. Baglin, M.F. Toney, H.F. Hamann, C.B. Murray, B.D. Terris, Journal of Physical Chemistry B 107 (2003) 5419.
[53] M. Chen, J.P. Liu, S. Sun, Journal of the American Chemical Society 126 (2004) 8394.
[54] S.R. Brankovic, J.X. Wang, R.R. Adzic, Electrochemical and Solid-State Letters 4 (2001) A217.
[55] S.R. Brankovic, N.S. Marinkovic, J.X. Wang, R.R. Adzic, Journal of Electroanalytical Chemistry 532 (2002) 57.
[56] K. Sasaki, J.X. Wang, M. Balasubramanian, J. McBreen, F. Uribe, R.R. Adzic, Electrochimica Acta (2004) 3873.
[57] H. Inoue, S.R. Brankovic, J.X. Wang, R.R. Adzic, Electrochimica Acta 47 (2002) 3777.
[58] K. Sasaki, Y. Mo, J.X. Wang, M. Balasubramanian, F. Uribe, J. McBreen, R.R. Adzic, Electrochimica Acta 48 (2003) 3841.
[59] J. Zhang, M.B. Vukmirovic, K. Sasaki, A.U. Nilekar, M. Mavrikakis, R.R. Adzic, Journal of the American Chemical Society 127 (2005) 12480.
[60] J. Zhang, M.B. Vukmirovic, Y. Xu, M. Mavrikakis, R.R. Adzic, Angewandte Chemie International Edition 44 (2005) 2132.
[61] M.B. Vukmirovic, J. Zhang, K. Sasaki, A.U. Nilekar, F. Uribe, M. Mavrikakis, R.R. Adzic, Electrochimica Acta 52 (2007) 2257.
[62] W.-P. Zhou, X. Yang, M.B. Vukmirovic, B.E. Koel, J. Jiao, G. Peng, M. Mavrikakis, R.R. Adzic, Journal of the American Chemical Society 131 (2009) 12755.
[63] Y. Xing, Y. Cai, M.B. Vukmirovic, W.-P. Zhou, H. Karan, J.X. Wang, R.R. Adzic, Journal of Physical Chemistry Letters 1 (2010) 3238.
[64] K.P. Gong, W.F. Chen, K. Sasaki, D. Su, M.B. Vukmirovic, W.P. Zhou, E.L. Izzo, C. Perez-Acosta, P. Hirunsit, P.B. Balbuena, R.R. Adzic, Journal of Electroanalytical Chemistry 649 (2010) 232.
[65] Y.C. Xing, Y. Cai, M.B. Vukmirovic, W.P. Zhou, H. Karan, J.X. Wang, R.R. Adzic, Journal of Physical Chemistry Letters 1 (2010) 3238.
[66] K. Sasaki, H. Naohara, Y. Cai, Y.M. Choi, P. Liu, M.B. Vukmirovic, J.X. Wang, R.R. Adzic, Angewandte Chemie International Edition 49 (2010) 8602.
[67] C. Koenigsmann, A.C. Santulli, K. Gong, M.B. Vukmirovic, W.-P. Zhou, E. Sutter, S.S. Wong, R.R. Adzic, Journal of the American Chemical Society 133 (2011) 9783.
[68] D. van der Vliet, C. Wang, M. Debe, R. Atanasoski, N.M. Markovic, V.R. Stamenkovic, Electrochimica Acta 56 (2011) 8695.
[69] C. Wang, D. van der Vliet, K.L. More, N.J. Zaluzec, S. Peng, S. Sun, H. Daimon, G. Wang, J. Greeley, J. Pearson, A.P. Paulikas, G. Karapetrov, D. Strmcnik, N.M. Markovic, V.R. Stamenkovic, Nano Letters 11 (2010) 919.

[70] C. Wang, M. Chi, D. Li, D. Strmcnik, D. van der Vliet, G. Wang, V. Komanicky, K.-C. Chang, A.P. Paulikas, D. Tripkovic, J. Pearson, K.L. More, N.M. Markovic, V.R. Stamenkovic, Journal of the American Chemical Society 133 (2011) 14396.
[71] Y. Chen, Z. Liang, F. Yang, Y. Liu, S. Chen, Journal of Physical Chemistry C 115 (2011) 24073.
[72] V. Mazumder, M. Chi, K.L. More, S. Sun, Journal of the American Chemical Society 132 (2010) 7848.
[73] G. Chen, D.A. Delafuente, S. Sarangapani, T.E. Mallouk, Catalysis Today 67 (2001) 341.
[74] J.L. Fernandez, J.M. White, Y. Sun, W. Tang, G. Henkelman, A.J. Bard, Langmuir 22 (2006) 10426.
[75] C.M. Sanchez-Sanchez, J. Rodriguez-Lopez, A.J. Bard, Analytical Chemistry 80 (2008) 3254.
[76] C.M. Sanchez-Sanchez, J. Solla-Gullon, F.J. Vidal-Iglesias, A. Aldaz, V. Montiel, E. Herrero, Journal of the American Chemical Society 132 (2010) 5622.
[77] S.E. Fosdick, R.M. Crooks, Journal of the American Chemical Society 134 (2011) 863.
[78] S. Guerin, B.E. Hayden, C.E. Lee, C. Mormiche, J.R. Owen, A.E. Russell, Journal of Combinatorial Chemistry 6 (2004) 149.
[79] S. Guerin, B.E. Hayden, C.E. Lee, C. Mormiche, A.E. Russell, Journal of Physical Chemistry B 110 (2006) 14355.
[80] T. He, E. Kreidler, L. Xiong, J. Luo, C.J. Zhong, Journal of the Electrochemical Society 153 (2006) A1637.
[81] T. He, E. Kreidler, Physical Chemistry Chemical Physics 10 (2008) 3731.
[82] J. Greeley, T.F. Jaramillo, J. Bonde, I. Chorkendorff, J.K. Nørskov, Nature Materials 5 (2006) 909.
[83] J. Greeley, J.K. Nørskov, Surface Science 601 (2007) 1590.
[84] J. Greeley, J.K. Nørskov, Journal of Physical Chemistry C 113 (2009) 4932.
[85] N.S. Froemming, G. Henkelman, Journal of Chemical Physics 131 (2009).
[86] S. Koh, P. Strasser, Journal of the American Chemical Society 129 (2007) 12624.
[87] Z. Liu, S. Koh, C. Yu, P. Strasser, Journal of the Electrochemical Society 154 (2007) B1192.
[88] R. Srivastava, P. Mani, N. Hahn, P. Strasser, Angewandte Chemie International Edition 46 (2007) 8988.
[89] P. Mani, R. Srivastava, P. Strasser, Journal of Physical Chemistry C 112 (2008) 2770.
[90] K.C. Neyerlin, R. Srivastava, C.F. Yu, P. Strasser, Journal of Power Sources 186 (2009) 261.
[91] R. Srivastava, P. Mani, P. Strasser, Journal of Power Sources 190 (2009) 40.
[92] P. Strasser, Reviews in Chemical Engineering 25 (2009) 255.
[93] S. Koh, P. Strasser, Journal of the Electrochemical Society 157 (2010) B585.
[94] P. Strasser, S. Koh, T. Anniyev, J. Greeley, K. More, C.F. Yu, Z.C. Liu, S. Kaya, D. Nordlund, H. Ogasawara, M.F. Toney, A. Nilsson, Nature Chemistry 2 (2010) 454.
[95] R.Z. Yang, J. Leisch, P. Strasser, M.F. Toney, Chemistry of Materials 22 (2010) 4712.
[96] F. Hasche, M. Oezaslan, P. Strasser, Chemcatchem 3 (2011) 1805.
[97] P. Mani, R. Srivastava, P. Strasser, Journal of Power Sources 196 (2011) 666.
[98] M. Oezaslan, P. Strasser, Journal of Power Sources 196 (2011) 5240.
[99] M. Oezaslan, M. Heggen, P. Strasser, Journal of the American Chemical Society 134 (2011) 514.
[100] R.Z. Yang, P. Strasser, M.F. Toney, Journal of Physical Chemistry C 115 (2011) 9074.
[101] F. Hasche, M. Oezaslan, P. Strasser, Journal of the Electrochemical Society 159 (2012) B25.
[102] M.R. Knecht, M.G. Weir, V.S. Myers, W.D. Pyrz, H.C. Ye, V. Petkov, D.J. Buttrey, A.I. Frenkel, R.M. Crooks, Chemistry of Materials 20 (2008) 5218.
[103] D.F. Yancey, E.V. Carino, R.M. Crooks, Journal of the American Chemical Society 132 (2010) 10988.
[104] E.V. Carino, R.M. Crooks, Langmuir 27 (2011) 4227.
[105] V.S. Myers, M.G. Weir, E.V. Carino, D.F. Yancey, S. Pande, R.M. Crooks, Chemical Science 2 (2011) 1632.
[106] S. Pande, M.G. Weir, B.A. Zaccheo, R.M. Crooks, New Journal of Chemistry 35 (2011) 2054.
[107] D.F. Yancey, L. Zhang, R.M. Crooks, G. Henkelman, Chem. Sci. (2012).
[108] M. Teliska, V.S. Murthi, S. Mukerjee, D.E. Ramaker, Journal of the Electrochemical Society 152 (2005) A2159.
[109] M. Tada, S. Murata, T. Asakoka, K. Hiroshima, K. Okumura, H. Tanida, T. Uruga, H. Nakanishi, S.-I. Matsumoto, Y. Inada, M. Nomura, Y. Iwasawa, Angewandte Chemie International Edition 46 (2007) 4310.
[110] E.A. Lewis, I. Kendrick, Q. Jia, C. Grice, C.U. Segre, E.S. Smotkin, Electrochimica Acta 56 (2011) 8827.
[111] J.A. Rodriguez, Surface Science Reports 24 (1996) 223.
[112] W.J. Tang, G. Henkelman, Journal of Chemical Physics 130 (2009).
[113] H.L. Xin, N. Schweitzer, E. Nikolla, S. Linic, Journal of Chemical Physics 132 (2010).
[114] M.C.S. Escano, H. Nakanishi, H. Kasai, Journal of Physical Chemistry A 113 (2009) 14302.
[115] Z. Yang, Y. Zhang, J. Wang, S. Ma, Physics Letters A 375 (2011) 3142.
[116] Z. Yang, Z. Geng, Y. Zhang, J. Wang, S. Ma, Chemical Physics Letters 513 (2011) 118.
[117] Z.X. Yang, J.L. Wang, X.H. Yu, Chemical Physics Letters 499 (2010) 83.
[118] J.J. Mateo, D.A. Tryk, C.R. Cabrera, Y. Ishikawa, Molecular Simulation 34 (2008) 1065.
[119] Y. Ishikawa, J.J. Mateo, D.A. Tryk, C.R. Cabrera, Journal of Electroanalytical Chemistry 607 (2007) 37.
[120] J.A. Santana, J.J. Mateo, Y. Ishikawa, Journal of Physical Chemistry C 114 (2010) 4995.
[121] L. Ou, F. Yang, Y. Liu, S. Chen, Journal of Physical Chemistry C 113 (2009) 20657.